Creep and Electrochemical Corrosion Behavior of Heat-treated Mg-9Al-1Zn Alloy

Ravi Naldi & Anawati Anawati*

Department of Physics, Faculty of Mathematics and Natural Sciences (FMIPA), Universitas Indonesia, Depok 16424, Indonesia
*E-mail: anawati@sci.ui.ac.id

Highlights:

- The heat treatment homogenized the β phase.
- The β phase was observed mainly at triple points of grain boundaries of the heat-treated alloy.
- The time to rupture was ten times longer for the heat-treated alloy than for the cast alloy.
- The polarization and EIS tests indicated a slight improvement in corrosion resistance of the heat-treated alloy relative to the untreated one.

Abstract. The high-strength Mg-9Al-1Zn alloy has been extensively investigated due to its potential application as a structural material in the automotive industry. The main challenges for its use are the low creep and corrosion resistance. In this work, heat treatment at 415 °C for 2 h was conducted on as-cast Mg-9Al-1Zn to improve its creep resistance. The corrosion behavior of the alloy was studied by the electrochemical method in an NaCl solution. The creep test results under 66.5 MPa load at 200 °C indicated one order of magnitude higher creep resistance of the heat-treated alloy relative to the as-cast one. The heat-treated specimen was ruptured after 6.5 h while the as-cast one was ruptured within 0.6 h. Creep occurred locally following the β phase in the alloy as evident from the cavities observed after the test. Reduction in the density of the discontinuous β precipitates resulting from heat treatment of the alloy lowered the susceptibility to creep. The smaller volume fraction of β precipitates suppressed the cathodic reaction during the polarization test and raised the electrochemical impedance spectra during the EIS test. The heat treatment improved not only the creep resistance but also the corrosion resistance of the Mg-9Al-1Zn alloy.

Keywords: *corrosion; EIS; creep; heat treatment; magnesium alloy; microstructure.*

1 Introduction

Magnesium (Mg) alloy exhibits low density, high strength to weight ratio, high castability, excellent damping ability, and outstanding recyclability, which make it suitable for application in the automotive industry [1]. Reduction in the structural weight of automobiles leads to lower energy consumption, which minimizes the release of gas pollutants. The binary Mg-Al system, such as the

Received October 14th, 2019, Revised January 13th, 2020, Accepted for publication July 31st, 2020.
 ISSN: 2337-5779,
DOI: 10.5614/j.eng.technol.sci.2020.52.5.1

AZ and AM series, is the most popular commercial Mg alloy for engineering applications [2]. The alloying elements Al, Zn, and Mn enhance the mechanical properties of Mg through the mechanism of precipitation hardening [1-4]. Apart from improving its hardness and strength, alloying Mg with Al, Zn and Mn improves its corrosion resistance [3,5]. Incorporation of the stable aluminum oxide raises the protectiveness of the oxide film on the alloy [5]. The ternary AZ91 alloy, which comprises 9 wt% Al and 1 wt% Zn as the primary alloying elements and a small addition (0.4 wt%) of Mn exhibits the highest strength and hardness among the other AZ series [1]. The amount of alloying element Al is limited by the maximum solubility of Al in Mg, which is 12.9 wt% at the eutectic temperature of 710 K [6]. The solubility decreases with temperature and reaches equilibrium concentration 2.9 wt% at 473 K. Reduction in the solubility leads to the formation of precipitation of the second phase, $Mg_{17}Al_{12}$, also known as β phase [1,6]. No other new phase is formed as long as the ratio of Al to Zn is higher than 3:1. In that case, Zn substitutes Al in the β precipitate, forming an intermetallic compound, $Mg_{17}Al_{11.5}Zn_{0.5}$ or $Mg_{17}(Al, Zn)_{12}$ [7]. The volume fraction of β precipitates plays a vital role in determining the mechanical behavior and corrosion performance of the alloy [7-12].

The microstructure of the AZ91 alloy is sensitive to heat treatment because of the variation in the solubility of the alloying element as a function of temperature. Segregation of discontinuous β precipitates occurs in AZ91 as a result of annealing at 423 K for 16 h, which leads to an increase in the ultimate compression strength while at a higher temperature of 623 K homogenization of the solid solution is caused, which increases the yield strength [7]. AZ91 containing a high density of β precipitates leads to a poor wear resistance as a result of stress concentration in the precipitate-matrix interface, which tends to generate cracks during friction [12]. Solution treatment (T4) followed by aging (T6) improves wear resistance, strength and hardness due to the formation of high-density dispersed fine β precipitate in the α-Mg matrix. Grain refinement as a result of the addition of alloying element Ca or rare earth element has been reported to be able to lock the creep displacement in the AZ91 alloy [13]. However, new phases are formed, which lower the corrosion resistance of the alloy. The precipitates are known to play a double role in the corrosion of Mg alloys, depending on their volume fraction [5]. They serve as micro-galvanic cathodes, which speed up the corrosion of the matrix or as a barrier to retard the propagation of corrosion. A network of continuous precipitates is more effective in stopping the development of corrosion, whereas a small amount of discontinuous precipitates accelerates corrosion. In this work, the effect of non-standard heat treatment at 415 °C for 2 h on the microstructure and the resulting creep and corrosion performance of the AZ91 alloy were investigated.

2 Experimental and Methods

2.1 Specimen Preparation

Mg-9Al-1Zn alloys were prepared by gravity casting from pure Mg, Al, and Zn scraps. The scraps were melted at 750 °C in an argon atmosphere and stirred with a graphite rod. The molten alloy was then poured into a cylindrical mold and cooled down to room temperature. Heat treatment was applied to a number of as-cast rod ingots with a diameter of 2 cm and a length of 10 cm. The heat treatment was conducted at 415 °C in an argon atmosphere for 2 h. The specimen was immediately quenched in water after the heat treatment. The ingot was then sliced into a 1-cm thick disk. The disk specimen was ground with #800, #1000, #1200 and #2000 grit paper and then polished by using alumina paste until giving a mirror finish. The specimen was degreased in acetone and ethanol before further use.

2.2 Surface characterization

The chemical composition of the as-cast and heat-treated alloys was analyzed by X-ray fluorescence spectroscopy (XRF). Table 1 lists the chemical composition of the as-cast and heat-treated alloys. The concentration of alloying elements Al and Zn was 9 ± 1 wt% and 1 ± 0.5 wt%, respectively, for both alloys.

Table 1 Chemical composition of the as-cast and heat-treated mg-9al-1zn alloys.

Elements	As-cast		Heat-treated	
	Wt%	At%	Wt%	At%
Al	8.71	7.96	10.18	9.35
Zn	0.87	0.33	1.42	0.54
Mg	90.42	91.71	88.41	90.11

Prior to microstructure observation, the specimens were etched in 4 vol% HNO_3 solution in ethanol for 20 s. The specimen was then washed with DI water and dried in an air stream before further investigation. The microstructure was studied with FE-SEM along with an EDS analysis (FEI Inspect F-50 and EDAX analyzer). The number of precipitates on the specimen was further analyzed using the ImageJ software.

2.3 Creep Test

A uniaxial creep test was performed based on an ASTM E 195 rod specimen with a diameter of 12 mm. The experiment was conducted at 200 °C under a 50-kg load using a creep test machine from SATEC SYSTEM INC. The fracture morphology was investigated by optical microscope (Zeiss).

2.4 Electrochemical Corrosion Test

The corrosion behavior of the specimen was evaluated by performing electrochemical tests: open circuit potential (OCP) measurement, potentiodynamic polarization test, and electrochemical impedance spectroscopy (EIS) using a potentiostat (Corrtest CS310); the electrochemical tests procedure followed the ASTM G5 standard [14]. The specimen was molded in resin to expose one surface only. The test used three-electrode configurations: platinum mesh as counter electrode, the specimen as working electrode, and silver/silver chloride (Ag/AgCl) as reference electrode. The test was carried out in 250 ml of 3.5 wt% NaCl solution.

The solution was stirred at a constant rate of 300 rpm using a magnetic stirrer and the temperature was kept at 30 °C ± 1 °C. For the potentiodynamic polarization test, the potential was swept at a speed of 0.5 mV/s from -100 mV below OCP to 100 mV above OCP. The corrosion potential and current density were determined from the polarization curve by the Tafel extrapolation method. The method is described in detail in Ref. [15]. The EIS data were collected by conducting the test at OCP, at a frequency range of 10^{-2} to 10^{5} Hz.

3 Results and Discussion

The microstructure of the Mg-9Al-1Zn alloy is displayed in Figure 1, together with the EDS point analysis results. The as-cast alloy was composed of α (Mg) decorated by α + β ($Mg_{17}Al_{12}$) phase (Figure 1(a)). The dendrite structure of the β phase existed both as continuous and discontinuous precipitates, which appeared as white particles segregated along the grain boundaries. The discontinuous precipitates were typically developed during slow cooling during solidification [1]. The EDS spectra in Figure 1 show the elemental composition of the precipitates and the metal matrix. The continuous precipitate consisted of Mg and Al with a concentration of 60 ± 2 wt% and 34 ± 1 wt%, respectively, as displayed in EDS analysis point 1. The molecular weight ratio of Mg to Al agreed well with the stoichiometric $Mg_{17}Al_{12}$ [6]. The β phase contained 4.48 wt% Zn. During solidification, Zn substituted Al in the β precipitate, creating ternary compound $Mg_{17}Al_{11.5}Zn_{0.5}$. The notation for the ternary compound is often simplified to $Mg_{17}Al_{12}$ [7]. The continuous precipitates exhibited a lath-shaped morphology as displayed in the higher magnification in Figure 1(a). Round-shaped β precipitates were also observed sporadically in the grain boundary of the as-cast alloy. The grain size of the matrix α phase in the as-cast alloy was in the order of 10-20 μm. Confirming the XRF result in Table 1, the EDS analysis at point 2 revealed that the matrix consisted of 9 ± 1 wt% Al and 1 ± 0.5 wt% Zn, which corresponds well to the AZ91 series alloy.

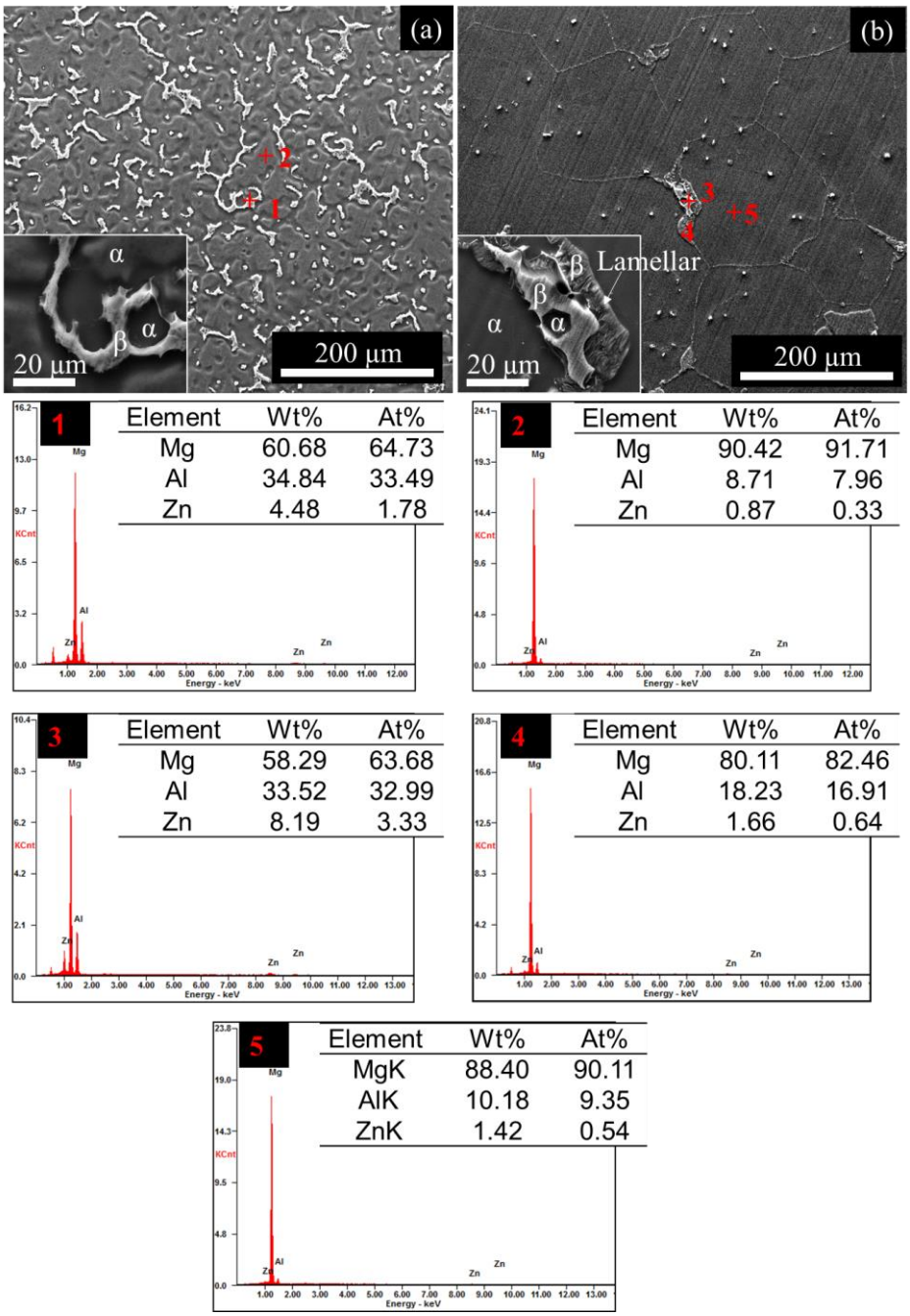

Figure 1 FE-SEM images showing the element distribution in the (a) as-cast and (b) heat-treated alloys and the corresponding EDS point analysis at points 1-5.

Figure 1(b) shows the microstructure of the Mg-9Al-1Zn alloy after the heat treatment. The grain became significantly larger, in the range of 100 to 200 μm. The enlargement of the grain size was accompanied by a reduction in the density of the precipitates. Homogenization of the Al in the matrix occurred during the high-temperature heat treatment. The remaining discontinuous precipitates were mostly located at the intersection points of the grain boundaries while some round-shaped precipitates were spread randomly in the subgrain boundaries. The β phase exhibited two morphologies with a lath structure surrounded by lamellar precipitate, as shown clearly in Figure 1(b). The lamellar precipitates contained less Al (EDS point 4) than the lath precipitates (EDS point 3). The matrix of the heat-treated specimen contained a higher Al content at 10.18 wt% compared to the matrix of the as-cast alloy (8.71 wt%). Some of the remaining β precipitates were observed at the triple point of the grain boundaries.

Triple points that contain high microstructural defects and low free energy are preferential sites for the nucleation of precipitates [16]. Discontinuous lamellar precipitates are typically formed during slow cooling after heat treatment [1]. The delay time during transfer of the specimen from the furnace to the quenching bath after heat treatment possibly induced the nucleation of lamellar precipitates. The number of particles counted with the ImageJ software was 1527 precipitates and 486 precipitates in Figure 1(a) and (b), respectively. The number of precipitates in the heat-treated specimen was three times lower, but the size was ten times larger than that in the as-cast specimen.

A uniaxial creep test was performed on a rod ingot of the as-cast and heat-treated specimens at a temperature of 200 °C. Table 2 shows the parameters used during the creep test. Under an identical applied load per area, the as-cast alloy ruptured after only 0.6 s while the heat-treated specimen withstood until 6.5 s. The results indicate that the heat treatment lowered the creep susceptibility of the alloy approximately ten times.

The occupancy of grain boundaries by the ductile phase of β precipitates accelerated the creep behavior of the as-cast alloy during the test. Reduction in the density of the precipitates in the heat-treated specimen significantly enhanced the creep resistance of the alloy. The β precipitate has a melting temperature of 437 °C, which is lower than that of the Mg matrix (650 °C) [6]. At elevated temperature, the β phase, which was located along the grain boundaries of the as-cast alloy, was softened and induced creep. In contrast, creep occurred in the heat-treated alloy only at triple points where a β precipitate was located. Reduction in the number of creep initiation sites extended the time to rupture. The volume fraction of the precipitates was a dominant factor in determining the creep behavior. Expansion of the grain size contributed to a minor degree to the creep resistance of the alloy.

Table 2 Creep test parameters and results.

Specimen	Diameter (mm)	Area (mm^2)	Load (MPa)	Rupture time (h)
As-cast	12.07	114.42	66.45	0.6
Heat-treated	12.15	115.94	66.57	6.5

Figure 2 shows an optical microscope image of a cross-section of the specimen after the creep test. The grain boundaries were the sites most affected by creep. Heat applied during the creep test may induce microstructural instability, triggering nucleation of precipitates [4]. The grain size of both alloys was relatively stable after the creep test. The as-cast alloy showed numerous fine voids, which are visible as dark branches along the grain boundaries. Cracks were initiated at the void and propagated along the nearest grain boundary following the continuous precipitate.

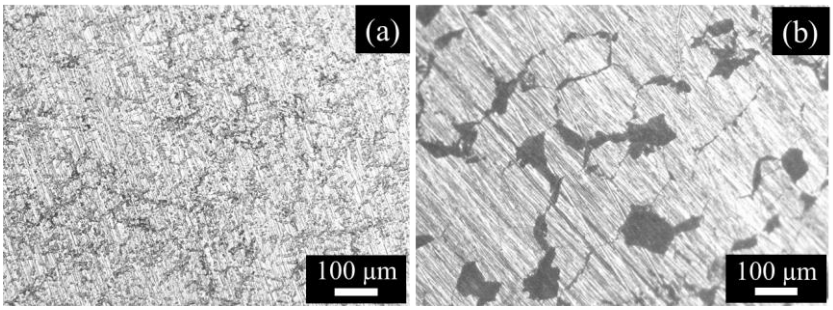

Figure 2 Optical microscope images of the (a) as-cast and (b) heat-treated alloy surfaces after the creep test.

Most of the observation area in Figure 2(a) was affected by creep. In contrast, the heat-treated alloy showed a smaller number of voids but with a larger size. The voids were localized mainly at the triple points of grain boundaries. Most of the grains remained unaffected by creep. The number of precipitates in the heat-treated alloy remained low and therefore exhibited higher creep resistance than the as-cast alloy. The coarsening of the β precipitates during the test was evident from the enlargement of the precipitates at the triple points.

The measured open circuit potential (OCP) and the potentiodynamic polarization curves of the as-cast and heat-treated specimens are shown in Figure 3. The OCP curve of the as-cast alloy displayed a slight decrease of potential from -1.52 to -1.53 $V_{Ag/AgCl}$, as shown in Figure 3(a). A slightly lower OCP value -1.54 to -1.55 $V_{Ag/AgCl}$ was obtained for the heat-treated specimens. The OCP curve for both alloys decreased with time, indicating continuous dissolution of the metal. The air-formed oxide layer on Mg alloys is not protective. Under exposure to the

corrosive solution, the Mg matrix, which was more anodic than the β precipitates, underwent corrosion. The corrosion product magnesium hydroxide may form as a result of hydrolysis with water. However, the compound is unstable at pH below 13 [17], especially when chloride ions are present. Therefore, the nature of corrosion products on magnesium metal surfaces is not protective. The OCP represents the corrosion potential of the metal matrix and is not sensitive to variation in the microstructure of the alloy.

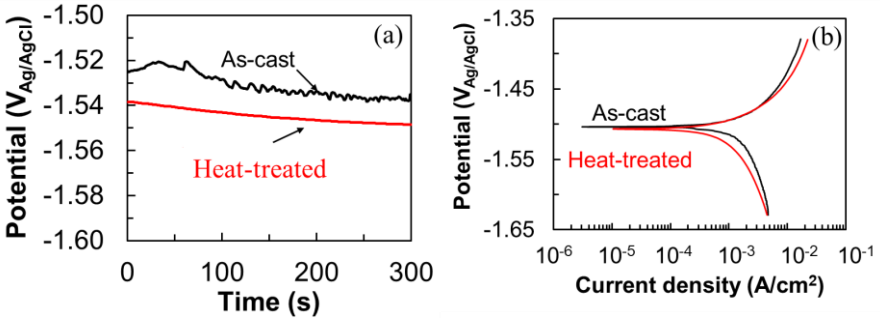

Figure 3 (a) Open circuit potential and (b) polarization curves of as-cast and heat-treated alloys in 3.5 wt% NaCl solution at 30 °C.

The potentiodynamic polarization test was more sensitive to the microstructure. Figure 3(b) shows that the heat treatment did not cause a significant shift in the polarization curve of the as-cast alloy. The corrosion potential of both the as-cast and the heat-treated specimen was the same at -1.50 $V_{Ag/AgCl}$. The value was similar to the corrosion potential reported for casted AZ91 alloy [5]. The anodic curve of the heat-treated alloy overlapped with the curve of the as-cast alloy. There was only a slight decrease in the cathodic current densities of the heat-treated alloy relative to the as-cast alloy, owing to the reduction of the number of cathodic precipitates (β phase). The corrosion current density decreased from 1.59×10^{-3} A/cm^2 in the as-cast specimen to 5.35×10^{-4} A/cm^2 in the heat-treated specimen. The corrosion resistance of the two-phase alloy was altered by the distribution of the second phase. In the as-cast alloy, the continuous precipitates became a corrosion barrier, but only for a short-range radius as the precipitates did not form a network at the grain boundaries. In the heat-treated alloy, discontinuous lamellar precipitates induced micro galvanic corrosion. The current densities produced by both specimens were similar, as shown by the overlapping anodic current curves. In agreement with the polarization test, the long-term corrosion behavior reported previously [18] showed an insignificant difference in the corrosion rate of the as-cast and the heat-treated alloy.

The change in surface resistivity as a result of the heat treatment was evaluated by EIS. Figure 4 shows the electrochemical impedance spectra of the as-cast and

heat-treated specimens in Nyquist, Bode and phase plots, including a fitted circuit model. The EIS spectra for the heat-treated specimen demonstrated a similar trend as the as-cast specimen but at a slightly higher value. The Nyquist plots of both specimens revealed two capacitive loops and one inductive loop, as shown in Figure 4(a). The diameter of the capacitive loop of the heat-treated alloy was slightly larger than that of the as-cast specimen, indicating higher corrosion resistance. In agreement with this, the heat-treated specimen exhibited a higher impedance and a higher phase angle at the frequency range 10^2 to 10^3 Hz, as shown in Figure 4(b) and (c). Figure 4(d) shows the fitted circuit represented electronic circuit model of the specimen surfaces. The fitted parameters, which are listed in Table 3, indicated no significant change of the surface resistivity between the as-cast and the heat-treated specimen. The faradaic and non-faradaic reactions on the surface were represented by constant phase elements (CPE_1 and CPE_2). The inductive loop in the fitted models of both alloys represents the susceptibility to pitting. Mg alloys containing precipitation are sensitive to localized corrosion owing to the galvanic coupling between the metal matrix and the precipitates [19]. The anodic phase (the metal matrix) corrodes while the cathodic phase (β phase) is protected. A reduction in the number of β precipitates following heat treatment suppresses the number of corrosion initiation sites.

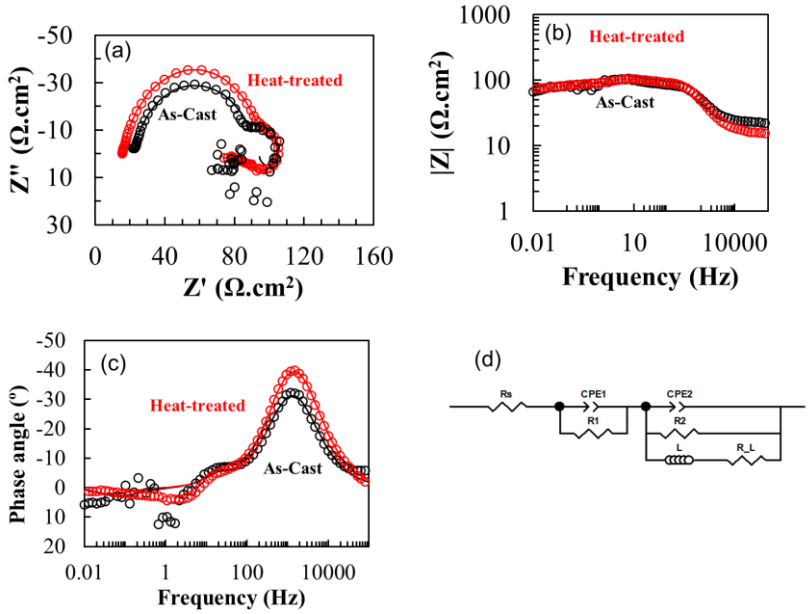

Figure 4 Electrochemical polarization data of as-cast and heat-treated alloys showing (a) Nyquist, (b) Bode impedance, (c) Bode phase plots, and d) the fitted circuit.

Table 3 Parameters of the fitted curve in the EIS spectra.

	R_s ($\Omega.cm^2$)	CPE_1 ($\Omega^{-1}.S^n.cm^{-2}$)	n_1	R_1 ($\Omega.cm^2$)	CPE_2 ($\Omega^{-1}.S^n.cm^{-2}$)	n_2	R_2 ($\Omega.cm^2$)	L (H)	R_L ($\Omega.cm^2$)
As-cast	22.35	$1.05x10^{-5}$	0.88	69.39	$1.76x10^{-4}$	1.24	12.56	10	3.14
Heat-treated	15.84	$9.02x10^{-6}$	0.89	82.55	$2.39x10^{-4}$	1.34	7.85	9	0.31

4 Conclusion

The influence of heat treatment on the creep and the electrochemical corrosion behavior of Mg-9Al-1Zn alloy were investigated. The creep resistance of the heat-treated alloy was remarkably improved, approximately ten times relative to the as-cast alloy. Surface characterization revealed that the as-cast alloy exhibited a high-volume fraction of the β phase, which existed as elongated precipitates, segregated along the grain boundaries. Enlargement of the metallic grain size about ten times and homogenization of the alloying element occurred as a result of the heat treatment. The number of β precipitates in the heat-treated alloy decreased approximately one third compared to that of the as-cast alloy. Reduction in the density of the precipitates enhanced the creep resistance of the alloy. It also decreased the cathodic current densities generated during the polarization measurement and increased the impedance value in the EIS spectra, indicating improvement of corrosion resistance. The results proved that the short-time heat treatment improved the creep resistance significantly without having an adverse effect on the corrosion performance of the alloy.

Acknowledgement

This research was supported by *Excellent Basic Research Grants for Higher Education, Ministry of Research Technology and Higher Education, Republic of Indonesia* (PDUPT DIKTI) under Contract No. NKB-1585/UN2.R3.1/HKP.05.00/2019. Thanks are due to Adi Ganda Putra for helping with the casting process.

References

[1] Pekguleryuz, M., Kainer, K. & Kaya, A., *Fundamentals of Magnesium Alloy*, Cambridge, United Kingdom, Woodhead Publishing Ltd., 2013.

[2] DeGarmo, E.P., Black, J.T. & Kohser, R.A., *Materials and Processes in Engineering*, 10th ed., Wiley, 2007.

[3] Hutchinson, C.R., Nie, J.F. & Gorsse, S., *Modeling the Precipitation Processes and Strengthening Mechanisms in A Mg-Al-(Zn) AZ91 Alloy*, Metall Mater Trans A Phys Metall Mater Sci., **36**, pp. 2093-105, 2005, DOI:10.1007/s11661-005-0330-x.

[4] Fatmi, M., Djemli, A., Ouali, A., Chihi, T., Ghebouli, M.A. & Belhouchet, H*., Heat Treatment and Kinetics of Precipitation of β-Mg17Al12 Phase in AZ91 Alloy*, Results Phys, **10**, pp. 693-698, 2018. DOI:10.1016/ j. rinp.2018.07.009.

[5] Lunder, O., Nordien, J.H. & Nisancioglu, K., *Corrosion Resistance of Cast Mg-Al Alloys*, Corros Rev, **15**, pp. 439-70, 1997. DOI:10.1515/ CORRREV.1997.15.3-4.439.

[6] Massalski, T., Okamoto, H., Subramanian, P. & Kacprzak, L., *Binary Alloy Phase Diagrams, 2nd ed.*, Materials Park, OH, United States, ASM, 1990.

[7] Braszczynska-Malik, K.N. & Kamicniaka, J., *Non-Standard Heat Treatment of Cast AZ91 Magnesium Alloy*, Archives of Foundry Engineering **8**(Special Issue 1), pp. 31-34, 2008.

[8] Srinivasan, A., Swaminathan, J., Gunjan, M.K., Pillai, U.T.S. & Pai, B.C., *Effect of Intermetallic Phases on the Creep Behavior of AZ91 Magnesium Alloy*, Mater Sci. Eng. A., **527**, pp. 1395-403, 2010. DOI: 10.1016/ j.msea.2009.10.008.

[9] Li, J., Jiang, Q., Sun, H. & Li, Y., *Effect of Heat Treatment on Corrosion Behavior of AZ63 Magnesium Alloy in 3.5 Wt.% Sodium Chloride Solution*, Corros Sci., **111**, pp. 288-301, 2016, DOI: 10.1016/j.corsci. 2016.05.019.

[10] Barylski, A., Kupka, M., Aniołek, K. & Rak, J., *The Effect of Precipitation Hardening on the Structure and Mechanical and Tribological Properties of Magnesium Alloy WE54*, Vacuum, **139**, pp. 77-86, 2017. DOI:10.1016/ j.vacuum.2017.02.015.

[11] Liu, Q., Ma, Q.X, Qiang, C.G., Cao, X., Zhang, S. & Luan, P.J., *Enhanced Corrosion Resistance of AZ91 Magnesium Alloy Through Refinement and Homogenization of Surface Microstructure by Friction Stir Processing*, Corros Sci., **138**, pp. 284-96, 2018. DOI:10.1016/ j.corsci.2018.04.028.

[12] Chen, Q., Li, K., Liu, Y., Zhao, Z., Tao, K. & Zhu, Q., *Effects of Heat Treatment on the Wear Behavior of Surfacing AZ91 Magnesium Alloy*, J. Mater Res., **32**, pp. 2161-2168, 2017. DOI:10.1557/jmr.2017.186.

[13] Jun, J.H., Park, B.K., Kim, J.M., Kim, K.T. & Jung, W.J., *Effects of Ca Addition on Microstructure and Mechanical Properties of Mg-RE-Zn Casting Alloy*, Mater Sci. Forum, **488-489**, pp. 107-110, 2005. DOI: 10. 4028/www.scientific.net/MSF.488-489.107.

[14] ASTM Standard G5-94, *Annu. B. ASTM Stand.*, pp. 54-64, 1997, DOI: 10.1520/G0005-94R11E01.

[15] Jones, D., *Principles and Prevention of Corrosion*, Mater Des., **14**(207), pp. 105-155, 1993.

[16] Hosford, W.F., *Physical Metallurgy, 2nd ed*., Boca Raton, FL: Taylor and Francis Group, 2010.

[17] Parsons, R., *Atlas of Electrochemical Equilibria in Aqueous Solutions*, J. Electroanal. Chem. Interfacial Electrochem, **13**(4), p. 471, 1967. DOI: 10.1016/0022-0728(67)80059-7.

[18] Naldi, R. & Anawati, A., *Effect of Solution Treatment on Microstructure and Corrosion Behaviour of Mg-9Al-1Zn Alloys*, IOP Conf. Ser. Mater Sci. Eng., **541**, International Seminar on Metallurgy and Materials 25-26 September 2018, Tangerang Selatan, Indonesia, 2019. DOI:10.1088/1757-899X/541/1/012008.

[19] Atrens, A., Liu, M. & Zainal Abidin, N.I., *Corrosion Mechanism Applicable to Biodegradable Magnesium Implants*, Mater Sci Eng B Solid-State Mater Adv. Technol., **176**, pp. 1609-1636, 2011 DOI:10.1016/j.mseb.2010.12.017.